

Magnetic reconnection and stochastic plasmoid chains in high-Lundquist-number plasmas

N. F. Loureiro,¹ R. Samtaney,² A. A. Schekochihin,³ and D. A. Uzdensky⁴

¹*Associação EURATOM/IST, Instituto de Plasmas e Fusão Nuclear — Laboratório Associado, Instituto Superior Técnico, Universidade Técnica de Lisboa, 1049-001 Lisboa, Portugal*

²*King Abdullah University of Science and Technology, Thuwal 23955, Saudi Arabia*

³*Rudolf Peierls Centre for Theoretical Physics, University of Oxford, Oxford OX1 3NP, UK*

⁴*Center for Integrated Plasma Studies, University of Colorado, Boulder CO 80309, USA*

(Dated: February 18, 2022)

A numerical study of magnetic reconnection in the large-Lundquist-number (S), plasmoid-dominated regime is carried out for S up to 10^7 . The theoretical model of Uzdensky *et al.* [Phys. Rev. Lett. **105**, 235002 (2010)] is confirmed and partially amended. The normalized reconnection rate is $\tilde{E}_{\text{eff}} \sim 0.02$ independently of S for $S \gg 10^4$. The plasmoid flux (Ψ) and half-width (w_x) distribution functions scale as $f(\Psi) \sim \Psi^{-2}$ and $f(w_x) \sim w_x^{-2}$. The joint distribution of Ψ and w_x shows that plasmoids populate a triangular region $w_x \gtrsim \Psi/B_0$, where B_0 is the reconnecting field. It is argued that this feature is due to plasmoid coalescence. Macroscopic “monster” plasmoids with $w_x \sim 10\%$ of the system size are shown to emerge in just a few Alfvén times, independently of S , suggesting that large disruptive events are an inevitable feature of large- S reconnection.

PACS numbers: 52.35.Vd, 94.30.Cp, 96.60.Iv, 52.35.Py

Introduction. It has become clear in recent years that resistive magnetic reconnection at asymptotically high Lundquist numbers (S) is a temporally and spatially irregular process, dominated by multiple plasmoids generated in unstable current sheets [1–8]. The reconnection rate in this regime is independent of S provided $S > S_c$ [6, 8], where $S_c \sim 10^4$ [9, 10] is the plasmoid instability [1] threshold. Thus, the classic Sweet-Parker (SP) theory [11, 12] is no longer sufficient even for resistive MHD reconnection and a new physical paradigm is needed.

Such a theory was recently attempted by [13] (henceforth ULS). The physical picture on which it is based is that, as the plasmoid instability [1] proceeds into its nonlinear stage, inter-plasmoid current sheets form, which are then subject to the same instability. The result is a multiscale plasmoid chain originally envisioned by [14]. ULS assume that (i) the current sheets connecting the plasmoids in this chain are typically just marginal with respect to the plasmoid instability and so their length is $\sim L_c = (\eta/V_A)S_c$, where η is the magnetic diffusivity and V_A the Alfvén speed based on the upstream magnetic field B_0 ; (ii) the reconnecting field is equal to the upstream field B_0 for all interplasmoid layers and so outflows into all plasmoids are Alfvénic with the same speed V_A ; and (iii) smaller plasmoids do not have time to saturate before they are ejected into larger ones (and are promptly merged with them). ULS then show that (i) the effective reconnection rate is $\tilde{E}_{\text{eff}} = cE_{\text{eff}}/B_0V_A \sim S_c^{-1/2} \sim 0.01$; (ii) the plasmoid flux (Ψ) and cross-sheet half-width (w_x) distribution functions are $f(\Psi) \sim \tilde{E}_{\text{eff}}B_0L\Psi^{-2}$ and $f(w_x) \sim \tilde{E}_{\text{eff}}Lw_x^{-2}$ (the power laws are the same because it is argued that $\Psi \sim w_xB_0$); and (iii) anomalously large “monster” plasmoids occasionally occur, with sizes $\sim S_c^{-1/4}L \sim 0.1L$,

where L is the system size. Note that diagnosing the plasmoid chain in terms of the flux and half-width distributions is a natural statistical description for such an object [13, 15, 16]. Note also that the prediction of monster plasmoids is potentially an important one in light of the evidence of violent abrupt events associated with reconnection sites (e.g., solar flares [17] or sawtooth [18]).

In this Letter, we present a numerical study of resistive MHD reconnection at the highest currently achievable Lundquist numbers. Our results confirm the basic predictions of the ULS theory, but also reveal that the picture is more complex than originally envisioned.

Numerical setup. We use the same numerical scheme as [5] to solve the standard set of compressible visco-resistive MHD equations in a 2D box $[-L_x, L_x] \times [-L_y, L_y]$. Our setup is designed so that a statistical steady state can be reached. Namely, the density, pressure and the incoming magnetic field are imposed at the upstream boundaries ($x = \pm L_x$): $\rho = 1$, $P = 3$ and $B_y = B_0 \{1 + \cos[(\pi y/2L + \epsilon)^2]\} / 2$, where the code units are based on $V_A = B_0/\sqrt{4\pi\rho} = 1$ and $L = 1$. The small perturbation $\epsilon = 0.06L_y/L$ is necessary to break the y -symmetry of the numerical set up and thus prevent the artificial lingering of plasmoids at the center of the sheet. Solenoidality is used to fix $\mathbb{B}_x/\bar{x} = -\mathbb{B}_y/\bar{y}$ at the upstream boundary. For the velocity at this boundary, we set $u_y/\bar{x} = 0$, whereas $u_x(x = \pm L_x)$ is obtained from the frozen-flux condition (the box is wide enough that the resistive term is negligible at $x = \pm L_x$). Free-outflow boundary conditions are imposed at the downstream ($y = \pm L_y$) boundaries. The initial condition is designed to mimic qualitatively a SP-like current sheet. This is not, however, a steady-state solution of the resistive MHD equations, so there is no need to add a pertur-

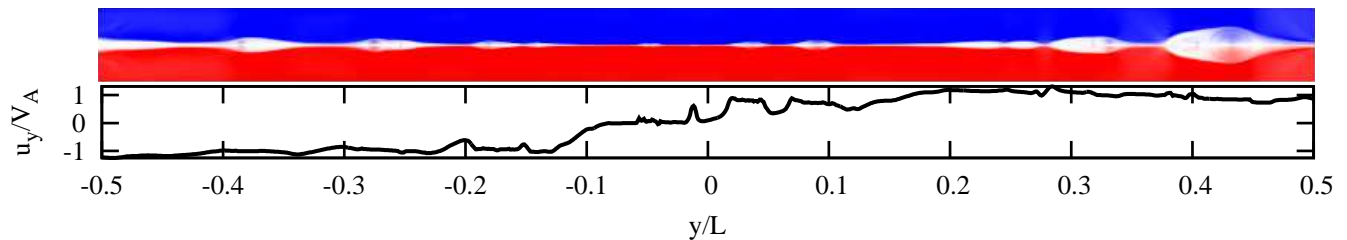


FIG. 1: Top panel: the plasmoid chain for the run with $S = 10^6$ (16384^2 grid points). Only a fraction of the x -domain is shown, $-0.03 \leq x/L \leq 0.03$. The color scale (blue to red) represents $B_y \in [-1, 1]$. Note that the assumption of ULS [13] that the reconnecting field is equal to the upstream field B_0 all the way to the thinnest of the current sheets appears to hold true. Bottom panel: outflow velocity $u_y(x=0, y)$. The outflows into most plasmoids are approximately Alfvénic.

bation to the initial configuration in order to trigger the plasmoid instability. The instability threshold for this setup is found to be $S_c \approx 1.2 \times 10^4$.

We perform a Lundquist-number scan in the range $300 \leq S \leq 10^7$. In all cases, the viscosity $\nu = \eta$. Most of our runs are done in a “semi-global” setup with $L_x = 0.3L$ and $L_y = 0.5L$; the exceptions, for lack of sufficient computational resources, are the runs with $S = 3 \times 10^6$ ($L_x = 0.15L$, $L_y = 0.25L$) and $S = 10^7$ ($L_x = 0.01L$, $L_y = 0.02L$) [25]. The numerical resolution depends on S , ranging up to 16384^2 for $S = 10^6$, 3×10^6 and 4096×8192 for $S = 10^7$ (for which the box is smaller).

Reconnection rate. In all our simulations with $S > S_c$, the initial SP-like configuration is quickly replaced with a plasmoid-dominated current sheet (Fig. 1). The system then enters a statistical steady state, with multiple plasmoids constantly being formed, coalescing and being ejected through the outflow boundary. We define the effective global reconnection rate in terms the inflow

plasma velocity at the upstream wall:

$$\tilde{E}_{\text{eff}} = \left\langle \frac{1}{2L_y V_A} \int dy u_x(x=L_x, y) \right\rangle, \quad (1)$$

where $\langle \dots \rangle$ denotes time average. This is plotted in Fig. 2 as a function of S . A transition is manifest from the SP scaling $\tilde{E}_{\text{eff}} \sim S^{-1/2}$ for $S \lesssim 10^4 \sim S_c$ to $\tilde{E}_{\text{eff}} \approx 0.02 \sim S_c^{-1/2}$, consistent with the ULS prediction [13] and previous numerical results [3, 4, 6–8]. Note that this result is now extended to larger values of S than ever before. Such an extension is important: as shown by ULS, $S \sim S_c^{3/2} \sim 10^6$ is the threshold at which an individual plasmoid can saturate faster than it is ejected from the global current sheet. This would slow down reconnection were it not for plasmoid ejection: smaller plasmoids are swallowed by larger ones before they have time to saturate. It was assumed by ULS that this coalescence process would operate efficiently — the persistence of fast reconnection beyond $S \sim 10^6$ demonstrated here suggests that this assumption is indeed valid.

Heating rate. The normalized resistive and viscous heating rates are $Q_\eta = \langle \int \int dx dy \eta j_z^2(x, y) / 2L_y B_0^2 V_A \rangle$, and $Q_\nu = \langle \int \int dx dy \nu \omega_z^2(x, y) / 2L_y V_A^3 \rangle$, where j_z and ω_z are the current and vorticity, respectively. These rates are also plotted in Fig. 2. In the fast-reconnection regime, $Q_\eta \approx Q_\nu \approx 0.008$. Since the total Poynting flux into the box is (per unit length) $P_{\text{in}} \approx 2\tilde{E}_{\text{eff}} \approx 0.04$ and the kinetic energy influx is small ($\propto u_x^3 \tilde{E}_{\text{eff}}^3$), the conclusion is that $\sim 40\%$ of the incoming (magnetic) energy is dissipated into heat (the rest goes into the reconnected field and the kinetic energy of the mass outflows).

Plasmoid distribution. The plasmoid population is naturally characterized by the distribution of fluxes (Ψ) and half-widths (w_x) of individual plasmoids [13, 15]. The distribution functions $f(\Psi)$ and $f(w_x)$ are plotted in Fig. 3. The Ψ^{-2} and w_x^{-2} scalings predicted by ULS do hold, although the distributions flatten for $\Psi/B_0 L$ and w_x/L below certain values that decrease at larger S .

A more detailed diagnostic is the joint distribution function $f(\Psi, w_x)$, which is shown in Fig. 4 and reveals a new feature: ULS argued that the plasmoid half-width and flux should be related by $w_x \sim \Psi/B_0$; in fact, there is a significant off-diagonal plasmoid population

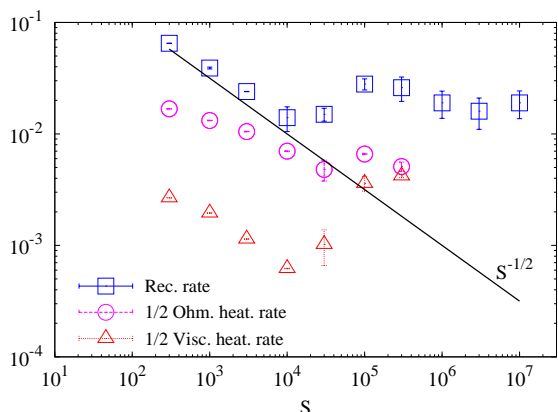


FIG. 2: Reconnection rate \tilde{E}_{eff} [Eq. (1), squares], and the (half) rates of resistive Q_η (circles) and viscous Q_ν (triangles) heating. Simulations with $S \geq 10^6$ last for shorter times before they are disrupted by monster ejections and so converged mean values for heating rates could not be obtained; the reconnection rate, calculated at the inflow boundary, did not have this problem.

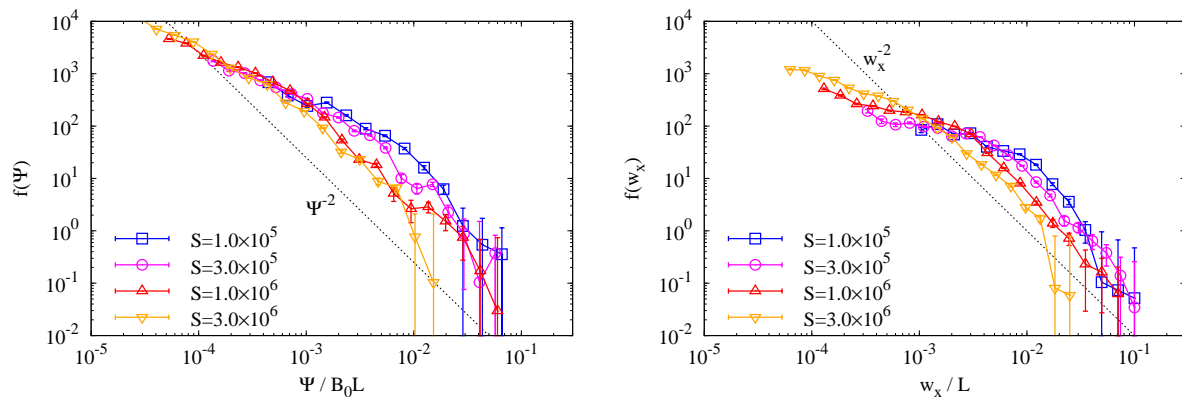


FIG. 3: Plasmoid flux (left) and half-width (right) distribution functions (note that the run with $S = 3 \times 10^6$ had a shorter box by half and so its distributions cut off at smaller flux and width). Dashed lines show the ULS scalings [13].

with $w_x > \Psi/B_0$ (cf. [15]). The presence of these plasmoids in the measured distribution can be explained as follows. The ULS argument assumed effectively that once a smaller plasmoid is ejected into a larger one, it is immediately and completely absorbed by (i.e., coalesces with) the latter and so falls out of the distribution. However, in reality, the coalescence between two plasmoids is not instantaneous (cf. [15]) — and so at any given time, there are many plasmoids for which coalescence has started at some earlier time and that are in an advanced stage of being digested by a bigger plasmoid. Thus, a typical plasmoid's life consists of two distinct phases: the ULS growth phase (while the plasmoid moves through its host current sheet) and the subsequent phase of digestion by a bigger plasmoid — this will have an effect on the plasmoid distribution.

We envision the coalescence as a gradual stripping of the outer layers of the smaller plasmoid so the magnetic field in a semidigested plasmoid is $B \sim B_0 w_x / w_{x0}$, where w_{x0} is the plasmoid's half-width at the beginning of the

coalescence [26]. Its flux is, therefore, $\Psi \sim B_0 w_x^2 / w_{x0}$. Since $w_x < w_{x0}$, these plasmoids are off-diagonal: $w_x > \Psi/B_0$. Fig. 5 illustrates the swallowing of a smaller plasmoid by a larger one; as shown in Fig. 4, the latter is relatively close to the diagonal, while the former is strongly off-diagonal.

Let us estimate the widths of the off-diagonal plasmoids. These have to be relatively small because larger plasmoids take a longer time to be digested and if that time exceeds the typical time $\tau_A \sim L/V_A$ for both predator and prey plasmoids to be ejected from the global sheet, then the effect on the measured distribution is small. The characteristic coalescence time is $t_{cl} \sim \Psi_0 / cE \sim B_0 w_{x0} / cE$, where Ψ_0 is the initial flux, $cE \sim V_A B_0 \max(S_c^{-1/2}, S_w^{-1/2})$ is the reconnection rate, $S_w \sim V_A w_{x0} / \eta$ is the Lundquist number associated with the (vertical) current sheet that forms between two coalescing plasmoids and we are taking into account that reconnection rate is independent of S_w for $S_w > S_c$, or $w_{x0} > L_c$ (length of the longest possible plasmoid-stable layer [13]; cf. [19]). Therefore, $t_{cl}/\tau_A \sim S_c^{1/2} (w_{x0}/L) \min(1, \sqrt{w_{x0}/L_c}) \lesssim 1$, or $w_{x0} \lesssim L \max(S_c^{-1/2}, S_c^{-1/3})$, is the condition for semidigested plasmoids to contribute to the off-diagonal part of the distribution. Since $\Psi \sim B_0 w_x^2 / w_{x0}$, this translates into

$$w_x/L \lesssim (\Psi/B_0 L)^{1/2} \max(S_c^{-1/4}, S_c^{-1/6}). \quad (2)$$

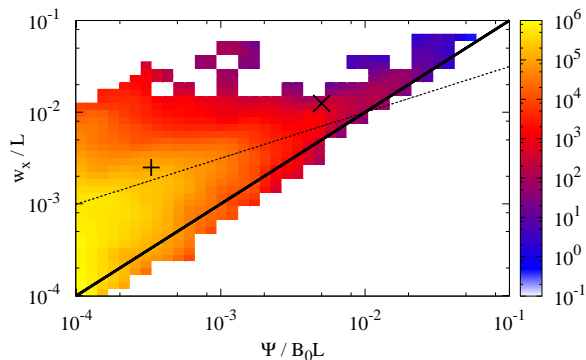


FIG. 4: Joint distribution of plasmoid flux and half-width for $S = 10^6$. The solid diagonal line shows the ULS plasmoids $w_x = \Psi/B_0$; the dotted line shows the condition (2). The predator and prey plasmoids shown in Fig. 5 are marked by \times and $+$, respectively.

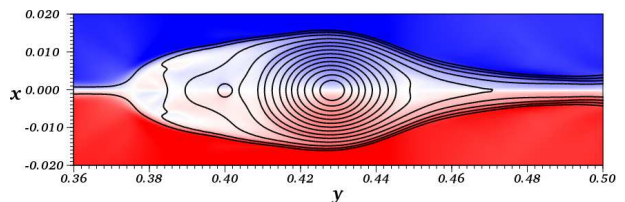


FIG. 5: Example of coalescing plasmoids: zoom on the rightmost part of Fig. 1. Same color scheme is used. Lines of constant magnetic flux are also shown.

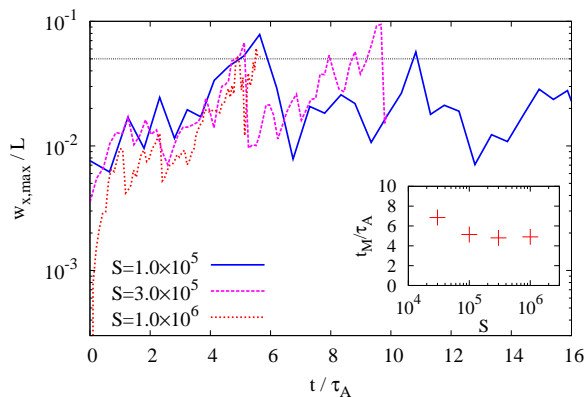


FIG. 6: The half-width of the largest plasmoid in the box vs. time. Time is measured from the start of steady-reconnection-rate phase. The dotted line is the monster threshold $0.05L$. Inset: time t_M to reach the monster threshold vs. S .

This indeed appears to capture the maximum of $f(\Psi, w_x)$ rather well (see Fig. 4 for $S = 10^6$; similarly good agreement was found for other values of S). Since (2) must be consistent with $w_x > \Psi/B_0$, the off-diagonal plasmoids only matter if $w_x/L \lesssim \max(S_c^{-1/2}, S^{-1/3})$. Note that the coalescence rate becomes independent of η for $S \gtrsim S_c^{3/2} \sim 10^6$.

Monster plasmoids. The following argument follows ULS [13], in a somewhat expanded and amended form. Because the flows carrying both flux and embedded plasmoids out of the current sheet are roughly linear, $u_y \sim V_{Ay}/L$ (see Fig. 1), the ejection time for a plasmoid born at some location y_0 in the sheet is $t_{ej} = \int_{y_0}^L dy/u_y \sim \tau_A \ln(L/y_0)$ (this is true both for the global sheet and also for any local one, in which case L would be the typical length for the latter). Therefore, plasmoids born near the center of the sheet remain in the game logarithmically longer than others. While this only leads to a logarithmic correction for their flux, $\Psi \sim \tilde{E}_{eff} V_A B_0 t_{ej} \sim \tilde{E}_{eff} B_0 L \ln L/y_0$, the enhancement of their area is much greater. A plasmoid grows in area by absorbing all the plasma and smaller plasmoids from roughly up to the midpoint of the layer that connects it to its neighbor of a similar size. One can then see that the plasmoid area A grows according to

$$\frac{dA}{dt} \sim \Delta y(t) \frac{d\Psi}{dt} \frac{\Psi}{B_0} \sim \Delta y(0) e^{t/\tau_A} \tilde{E}_{eff} V_A, \quad (3)$$

where $\Delta y(t)$ is the (exponentially stretched) half-distance to the neighboring plasmoid. Integrating (3) up to $t = t_{ej}$ gives $A(t_{ej}) \sim \tilde{E}_{eff} \Delta y(0) L(L/y_0 - 1)$.

If the plasmoid was born away from the center of the sheet, $y_0 \sim L$, then $A \sim \tilde{E}_{eff} \Delta y(0) L$ and so $w_x \sim A/w_y \sim \tilde{E}_{eff} L \sim 0.01L$. We have estimated the y -extent of the plasmoid as $w_y \sim \Delta y(0)$, which does not change as long as $w_x < w_y$. In contrast, for centrally born plasmoids, $y_0 \ll L$, we have $w_x \sim \tilde{E}_{eff} L^2/y_0$ at ejection,

provided $w_x < w_y \sim \Delta y(0)$. If the latter condition is not satisfied, i.e., if $y_0 < \tilde{E}_{eff} L^2/\Delta y(0)$, the plasmoid will be circularized as soon as $w_x \sim w_y$ (which will happen before ejection) and so its half-width at ejection will be $w_x \sim \tilde{E}_{eff}^{1/2} L(\Delta y(0)/y_0)^{1/2}$. Since $\Delta y(0) \leq y_0$, the maximum half-width achievable is $w_{x,max} \sim \tilde{E}_{eff}^{1/2} L \sim 0.1L$. This is a nearly macroscopic size — the plasmoids that reach it were dubbed *monster plasmoids* by ULS. Only those plasmoids stand a chance of achieving monster status that are born at $y_0 < \tilde{E}_{eff}^{1/2} L \sim 0.1L$. This must be consistent with $y_0 \gtrsim L_c$ (shorter sheets are stable), which implies that monsters will only appear if $S \gtrsim S_c^{5/4} \sim 10^5$.

Fig. 6 shows the half-width of the largest plasmoid, $w_{x,max}$ in the simulation box vs. time. Exponential growth to the monster size is manifest — this is defined here, somewhat arbitrarily, as $w_{x,max} = 0.05L$ ($0.1L$ is never actually reached in our simulations, but it is, of course, no more than an order-of-magnitude estimate; also our simulation domain is smaller than the system size, $L_y < L$). This size is usually achieved by just one plasmoid at a time, just before it is ejected, whereupon $w_{x,max}$ dips, then recovers as a new monster emerges, and so on. The time t_M for a plasmoid system to produce and grow a monster can be estimated simply as the ejection time for a plasmoid born in the relevant central part of the sheet: $t_M \sim t_{ej} \sim \tau_A \ln \tilde{E}_{eff}^{-1/2}$, which amounts to a few Alfvén times, independent of S — this is borne out by the numerical results (Fig. 6, inset). For monster plasmoids, $\Psi < B_0 w_x$ (like for the coalescing ones), so they occupy the top right corner of the (Ψ, w_x) plane in Fig. 4 (note that the large plasmoid in Fig. 5 is a monster in the making). The probability of finding a monster (defined by $w_x > 0.05L$) hovers between 1% and 3%.

Conclusions. We have found that resistive MHD reconnection is fast, its rate $cE/B_0 V_A = \tilde{E}_{eff} \sim 0.02$, independently of S . While a similar conclusion has been reported before [3, 4, 6–8], our study is the first to probe Lundquist numbers significantly exceeding the critical threshold of 10^6 [13] in order to show that plasmoid saturation does not shut down fast reconnection in the high-Lundquist-number, plasmoid-mediated regime. It also confirms that reconnection occurs via a multiscale plasmoid chain [13–15, 19], characterized by local Alfvénic outflows and many coalescing plasmoids.

Statistics of this “plasmoid turbulence” are measured for the first time in terms of the flux-width joint distribution — a natural choice both from the theoretical [13, 15] and observational [16] perspective. The ULS scalings $w_x \sim \Psi/B_0$, $f(\Psi) \sim \Psi^{-2}$, $f(w_x) \sim w_x^{-2}$ are corroborated, but we also find a substantial “off-diagonal” ($w_x > \Psi/B_0$) plasmoid population for $w_x \lesssim \tilde{E}_{eff} L$. The excess of plasmoids of relatively large size and small flux is explained by considering the coalescence between plasmoids. Thus, the full picture of the plasmoid “turbulence” involves not just multiple reconnection sites along

the global layer, but also many transverse layers between coalescing plasmoids (these layers can themselves break up into plasmoid chains [19]).

Another large-size low-flux subspecies is the “monster” plasmoids, also theoretically anticipated by [13]. They are born in the middle tenth of the global layer and grow to nearly macroscopic size in just a few Alfvén times, independently of the Lundquist number. This inevitable and relatively frequent nature of what can be very violent and disruptive events (ejection of a monster from the global layer) is reminiscent of the observed bursty character of plasmoid ejections in solar flares [17, 20] and perhaps also of the sawtooth crash in tokamaks [18].

These results show that even 2D MHD resistive reconnection contains a wealth of strongly nonlinear, stochastic behavior — a type of MHD turbulence that is only now starting to be studied quantitatively. It is encouraging that the simple phenomenology of the ULS model [13] appears to capture some of the essential properties of such systems, but it is also now clear that the full picture will require a deeper and more quantitative understanding of plasmoid coalescence and of the extreme events such as the emergence of monsters. Finally, many further complications will have to be taken into account before idealized models can truly describe the real-world reconnection in its full splendor: e.g., kinetic physics [3, 21, 22], background turbulence [4, 23], 3D effects [21, 24]).

Acknowledgments. This work was supported by Fundação para a Ciência e Tecnologia and by the European Communities under the contract of Association between EURATOM and IST (NFL), STFC (AAS), and by the Leverhulme Network for Magnetized Plasma Turbulence. The views expressed herein do not necessarily reflect those of the European Commission. Simulations were carried out at HPC-FF (Juelich), Jugene (Juelich; PRACE grant PRA024), Ranger (NCSA) and IBM Blue Gene Shaheen (KAUST).

- [3] W. Daughton et al., Phys. Rev. Lett. **103**, 065004 (2009).
 [4] N. F. Loureiro et al., Mon. Not. R. Astron. Soc. **399**, L146 (2009).
 [5] R. Samtaney et al., Phys. Rev. Lett. **103**, 105004 (2009).
 [6] A. Bhattacharjee et al., Phys. Plasmas **16**, 112102 (2009).
 [7] P. A. Cassak et al., Phys. Plasmas **16**, 120702 (2009).
 [8] Y. Huang and A. Bhattacharjee, Phys. Plasmas **17**, 062104 (2010).
 [9] D. Biskamp, Phys. Fluids **29**, 1520 (1986).
 [10] N. F. Loureiro et al., Phys. Rev. Lett. **95**, 235003 (2005).
 [11] P. A. Sweet, in *Electromagnetic Phenomena in Cosmical Physics*, edited by B. Lehnert (1958), vol. 6 of *IAU Symposium*, p. 123.
 [12] E. N. Parker, J. Geophys. Res. **62**, 509 (1957).
 [13] D. A. Uzdensky et al., Phys. Rev. Lett. **105**, 235002 (2010).
 [14] K. Shibata and S. Tanuma, Earth Planets Space **53**, 473 (2001).
 [15] R. L. Fermo et al., Phys. Plasmas **17**, 010702 (2010).
 [16] N. Nishizuka et al., Astrophys. J. **694**, L74 (2009).
 [17] J. Lin et al., Astrophys. J. **622**, 1251 (2005).
 [18] H. K. Park et al., Phys. Rev. Lett. **96**, 195003 (2006).
 [19] M. Bárta et al., arXiv:1011.4035 (2010).
 [20] M. Karlický and B. Kliem, Solar Phys. **266**, 71 (2010).
 [21] W. Daughton et al., Nature Phys. **7**, 539 (2011).
 [22] H. Karimabadi et al., Phys. Rev. Lett. **107**, 025002 (2011).
 [23] A. Lazarian and E. T. Vishniac, Astrophys. J. **517**, 700 (1999).
 [24] G. Lapenta and L. Bettarini, Europhysics Letters **93**, 65001 (2011).
 [25] Even in this case, the box is still much wider (in x) than the thickness of the SP layer, $\delta_{\text{SP}}/L \sim S^{-1/2} \sim 3 \times 10^{-4}$, and much longer (in y) than $L_c/L \sim S_c/S \sim 10^{-3}$.
 [26] When a typical plasmoid is ejected from its host layer into a bigger plasmoid, it is long and thin: $w_x \sim w_y \tilde{E}_{\text{eff}}$ [13]. However, immediately upon ejection, it is squashed against the bigger plasmoid and becomes circularized ($w_x \sim w_y$), while preserving its flux and area. Thus, just before it starts coalescing with the bigger plasmoid, its width jumps up by a factor of $\tilde{E}_{\text{eff}}^{-1/2} \sim 10$, and its magnetic field becomes $B_0 \tilde{E}_{\text{eff}}^{1/2}$ to preserve flux. This immediately moves the plasmoid vertically upwards by a factor $\tilde{E}_{\text{eff}}^{-1/2}$ from the ULS diagonal. Our arguments can be modified to account for this effect — the result is to raise the threshold (2) upwards by a factor of order unity.

[1] N. F. Loureiro et al., Phys. Plasmas **14**, 100703 (2007).

[2] G. Lapenta, Phys. Rev. Lett. **100**, 235001 (2008).